

MIMO CAPABILITY OF A MINIATURISED ANTENNA ARRAY WITH A DECOUPLING AND MATCHING NETWORK

Jörn Weber, Giovanni Del Galdo, Christian Volmer, Martin Haardt, Matthias A. Hein

Technische Universität Ilmenau, Institute for Information Technology
P.O. Box 100565, 98684 Ilmenau, Germany

ABSTRACT

We propose and evaluate an antenna array consisting of three, quarter-wavelength spaced, monopoles and a passive network. The latter decouples and matches the antenna array to prevent gain reduction. At the same time, it forms orthogonal radiation patterns, which divide the space into three different sections. By using a geometry-based channel model, the *Ilm-Prop*, we are able to quantify the improvement of the channel capacity and the bit error rate provided by the passive network with respect to the array without network under realistic conditions.

1. INTRODUCTION

Modern systems in wireless communications are expected to exploit spatial or pattern diversity, to enhance the quality and the capacity of communication channels. Such, so-called multiple input multiple output (MIMO) systems require antenna arrays consisting of p radiating elements. These p elements lead to $p - 1$ degrees of freedom to synthesise a desired radiation pattern by applying appropriate feeding currents to the antenna ports. Increasing the number of radiators not only increases the number of degrees of freedom but also the physical dimensions of the antenna. This represents a drawback for the use of smart antennas in small mobile platforms. Placing individual radiators closer together aggravates the problem of mutual coupling between antenna ports: power fed into the array ports is increasingly reflected towards the generator and thus cannot be radiated into space, i.e., the array becomes less efficient. We have demonstrated a method to decouple and match a miniaturised antenna array in [1, 2]. Here, we show that the orthogonality of the radiation patterns leads to an effective improvement of the channel capacity and the bit error rate (BER) under realistic MIMO scenarios.

2. MINIATURISED ANTENNA ARRAY

The proposed uniform linear array (ULA) consists of three monopoles designed for 1 GHz, which are separated by one quarter of a wavelength, i.e., 75 mm (Figure 1). The ground plane is $(0.5 \times 0.5) \text{ m}^2$ in size, to reduce problems due to

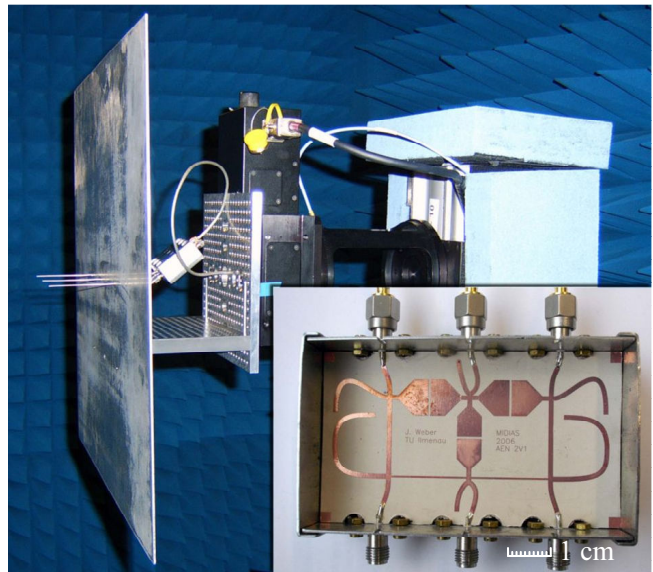


Fig. 1. Photographs of the antenna array and the decoupling and matching network.

experimental characterisation and excitation of the cross polarisation. The length of the monopoles has been optimised via the eigenmode matching approach presented in [2]. It has been shown that an antenna array can be analysed by means of the antenna eigenmodes, which correspond to the intrinsic degrees of freedom of the antenna array. Furthermore it has been clarified by measurements that the monopole length of 70 mm leads to a maximal matching of the worst eigenmode and is consequently the best choice.

The mathematical framework for the design of the decoupling and matching network (DMN) has been published in [1]. This method allows us to derive orthogonal beams with patterns close to desired ones. After the orthogonal patterns have been determined, the parameters of the DMN are defined. A major step towards a realisable topology was a successful elimination of 8 network elements [2]. On this account the DMN consists of 13 network elements instead of 21. The network elements have been implemented as quasi-lumped elements applying a standard printed circuit board

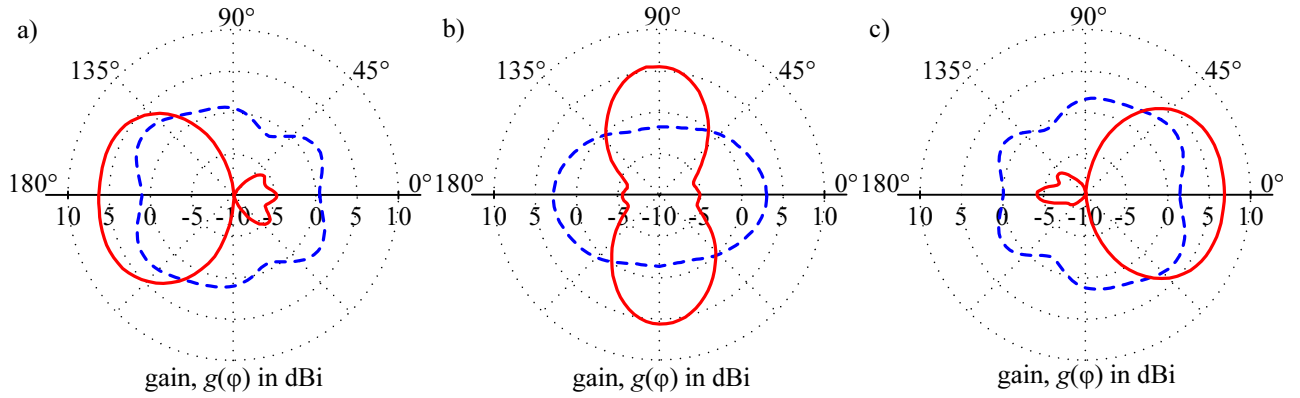


Fig. 2. Measured radiation patterns of the antenna system in the azimuth-plane at an elevation $\vartheta = 30^\circ$. The plots of the first (a), second (b) and third (c) port are normalised to a lossless isotropic radiator. The **dashed** lines represent the antenna without DMN, and the **solid** lines illustrate the patterns resulting from the antenna array including the designed DMN. The plotted dynamic range is 20 dB. The polarisation is vertical.

(PCB) process. The RO3203 high-frequency laminate [3] was used as substrate, with a dielectric constant of $\epsilon_r = 3.02$ and specified losses of $\tan \delta = 0.0016$. A photograph of the manufactured DMN is depicted in the inlay of Figure 1.

In Figure 2, the measured radiation patterns of the antenna array with and without DMN are compared. The plots are normalised to a lossless isotropic radiator by comparison with a measured standard gain horn antenna. The port patterns without DMN are distorted due to mutual coupling whereas the patterns of the array with DMN subdivide the space in three different sections. This separation was desired in the design process to make switched beam applications possible. It is apparent that the port patterns of the array with DMN achieve a higher maximum gain. A detailed enumeration of the maximum gains for the different patterns are depicted in Table 1. For comparison, a third array has been included, obtained by removing the center antenna element and therefore

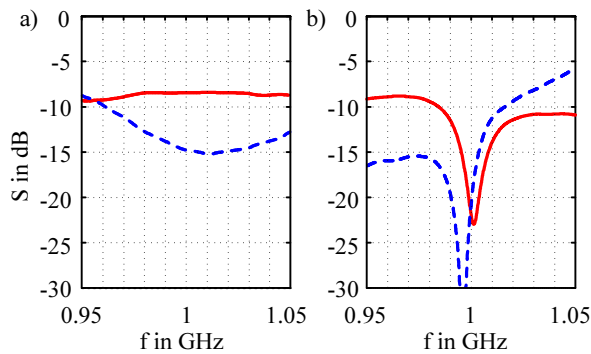


Fig. 3. Two representative scattering parameters S_{11} (**dashed** line) and S_{12} (**solid** line) of the antenna without DMN (a) and with DMN (b). The other parameters show similar behaviour and have been omitted for clarity.

antenna	η	g_{\max}	d_{\max}
3-ULA w/ DMN (a)	0.64	4.6/6.6 dB	7.1/8.5 dB
3-ULA w/ DMN (b)	0.64	3.7/5.6 dB	5.7/7.6 dB
3-ULA w/ DMN (c)	0.65	4.8/6.8 dB	7.4/8.7 dB
3-ULA w/o DMN (a)	0.63	2.3/3.5 dB	3.6/5.5 dB
3-ULA w/o DMN (b)	0.52	2.0/3.0 dB	3.8/5.8 dB
3-ULA w/o DMN (c)	0.65	2.4/3.8 dB	3.7/5.7 dB
2-ULA $\lambda/2$ (a)	0.76	2.3/3.7 dB	3.1/4.9 dB
2-ULA $\lambda/2$ (b)	0.77	2.4/3.9 dB	3.2/5.1 dB

Table 1. Antenna efficiency η , antenna gain g_{\max} , and antenna directivity d_{\max} for the antennas of the arrays under study.

consisting of two antennas $\lambda/2$ spaced.

The measured frequency response of the antenna system is depicted in Figure 3. The measurements demonstrated the successful operation of the DMN over a bandwidth of approximately 20 MHz. Only two representative scattering parameters are shown while the others show similar behaviour and have been omitted for clarity.

Table 1 not only shows the maximum gain of each port pattern for the different examples, but also the corresponding efficiencies η and directivities d_{\max} . The maximal gains g_{\max} have been measured relative to a standard gain horn antenna, while the directivities have been calculated by $d_{\max} = g_{\max}/\eta$. The efficiency η has been computed as the ratio of the radiated power to the power fed into the antenna system port, thus accounting for the total losses of the antenna. For this computation a surface integral had to be computed numerically. To obtain higher precision, such integrals have been computed as suggested in [4].

The results show comparable values for both three element ULAs and slightly better ones for the two element refer-

ence antenna. It is necessary to discuss these values in more detail, because there are different kinds of losses involved which should be considered. On one hand, dissipative losses in the antenna elements and the DMN reduce the radiated power and the efficiency. On the other hand, mutual coupling and mismatch lead to reflections of the incident power and consequently to a decreased efficiency. Thanks to the good matching and decoupling in the proposed array with DMN, the losses are mainly dissipative and reflections play a subordinated role. The array without DMN behaves vice versa: due to the absence of the DMN the amount of dissipative losses is lower in contrast to reflection losses.

Another relevant point is that the efficiency depends on the excitation vector and therefore on the synthesised pattern. It can be shown that for small element spacing, excitation of more directive patterns causes more difficulties with both, dissipative and reflective losses. To perform a comparison for similar excitations, the worst-case efficiency (η_w) of both examples is calculated. This worst-case efficiency appears by excitation of the weakest array eigenmode [2]. In this case both corresponding patterns have the same shape and the efficiencies are comparable. The resulting values are: $\eta_w = 56\%$ in case with DMN and $\eta_w = 21\%$ in case without DMN. The proposed array with DMN clearly outperforms the array without DMN with respect to the worst-case efficiency.

Not only the possible antenna gain is important for the application of an antenna array in a MIMO scenario, but also the orthogonality of the patterns. To quantify the degree of orthogonality of the patterns, the envelope correlation ρ_e has been analysed, which can be computed by the integration of the measured radiation patterns $\vec{F}_k(\Omega)$ over the solid angle Ω [5, 6]:

$$\rho_{ei,j} = \frac{\left| \oint \vec{F}_i(\Omega)^H \vec{F}_j(\Omega) d\Omega \right|^2}{\oint |\vec{F}_i(\Omega)|^2 d\Omega \oint |\vec{F}_j(\Omega)|^2 d\Omega}.$$

The superscript H designates the Hermitian transpose. The resulting correlation coefficients are:

Array	$\rho_{e1,2}$	$\rho_{e2,3}$	$\rho_{e1,3}$
3-ULA $\lambda/4$ w/o DMN	0.13	0.15	0.06
3-ULA $\lambda/4$ w/ DMN	0.02	0.03	0.01

The data confirm that the DMN decorrelates the antenna patterns, promising an improvement in diversity gain.

To summarise, we can state that the antenna array with DMN promises an advantage in MIMO scenarios due to higher antenna gains and to more orthogonal patterns [6].

3. PERFORMANCE OF THE ARRAY IN A MIMO SYSTEM

In order to investigate the impact of the DMN on the antenna performance in a realistic mobile communications system, the

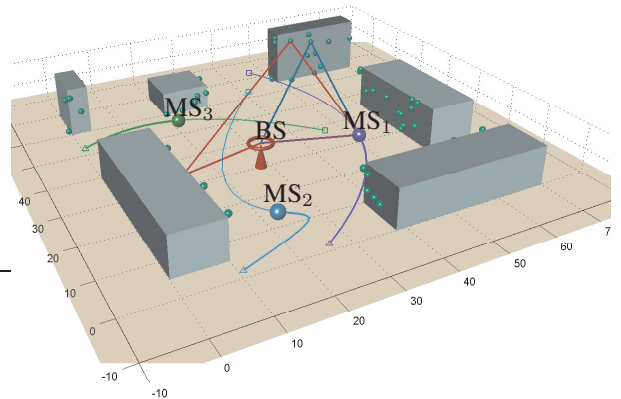


Fig. 4. Sample scenario generated with the *IlmProp* to illustrate the capabilities of the channel model. Three mobiles (MS_1 , MS_2 , and MS_3) move around a base station (BS). The scenario include point-like scatterers and obstacles (such as buildings), which can obstruct the propagation paths.

array with and without DMN has been compared in synthetic scenarios generated with the help of the *IlmProp* [7]. *IlmProp* is a flexible geometry-based Multi-User MIMO channel modeling tool, capable of dealing with time variant frequency selective scenarios. Figure 4 illustrates the capabilities of the *IlmProp*. Three mobiles (MS_1 , MS_2 , and MS_3) move around a base station (BS). Their curvilinear trajectories are shown. The BS and mobile terminals can employ any number of antennas arranged in an array of arbitrary geometry. The channel is computed as a sum of the line-of-sight (LOS) and of a number of rays which represent multi-path components (MPCs). The latter are obtained by point-like scatterers, which can be placed at will. The model supports both single and multiple reflections. In Figure 4, the LOS for MS_1 , a single bounce ray, and a double bounce ray are shown. The information about where the scatterers are, and how the paths are linked to them can be set arbitrarily, or it can be derived from high resolution parameter estimation from channel measurements. The information about the scenario is stored in form of Cartesian coordinates and their evolution in time. The scenario may include obstacles (such as buildings), which can obstruct the propagation paths. Furthermore, the *IlmProp* scenario can include real antenna arrays by means of measured radiation patterns.

3.1. Theoretical Scenario

At first, a scenario has been generated which mimics Jakes' assumptions for a Rayleigh channel [8]. A large number of scatterers (i.e., 100) are placed on a sphere surrounding the array under test. Outside the sphere one single antenna acts as the receiver. The scatterers provide a single bounce reflection and a random polarisation status. In this environment rich of

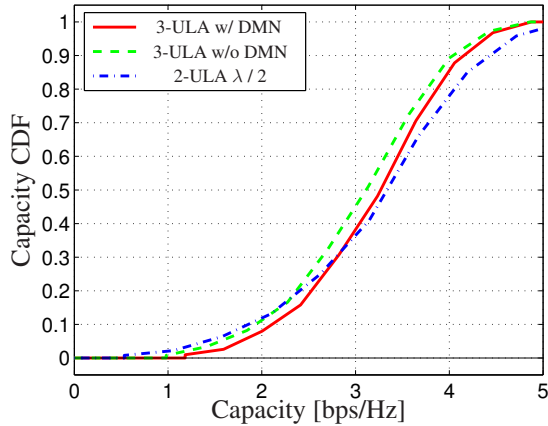


Fig. 5. Cumulative Distribution Function (CDF) of the capacity at an signal to noise ratio (SNR) of 10 dB for the antenna arrays under study.

MPCs, we can compute the correlation coefficient $\rho_{i,j}$ as

$$\rho_{i,j} = \left| \frac{E[h_i h_j^*]}{\sqrt{(E[|h_i|^2]) (E[|h_j|^2])}} \right|, \quad (1)$$

where h_i and h_j are the channel coefficients for the i -th and j -th antenna, respectively, and the superscript * denotes complex conjugation. The average has been performed across 500 realizations of the channel. Each realization has been characterised by random new positions of the scatterers on the sphere. The following table lists the correlation coefficients for the proposed array with DMN, without DMN, and for the third array consisting of two antennas spaced at $\lambda/2$. Note that the absolute value of the correlation depends on the number of MPCs.

Array	$\rho_{1,2}$	$\rho_{2,3}$	$\rho_{1,3}$
3-ULA w/ DMN	0.13	0.11	0.08
3-ULA w/o DMN	0.37	0.35	0.22
2-ULA $\lambda/2$	0.04	-	-

The values for ρ confirm that the use of the DMN effectively decorrelates the antennas by making the radiation patterns more orthogonal to each other, i.e., the energy is collected from different directions and, consequently, from different MPCs. In order to evaluate quantitatively the benefit offered by the proposed array with respect to the array without DMN, the cumulative distribution functions (CDF) of the capacity have been computed for the scenario mentioned above. To do so, it has been assumed that the arrays are used as transmitters and the available transmit power is fixed. The capacity C has been derived by the following equation [9]:

$$C = \log_2 \left(\det \left(\mathbf{I} + \frac{\gamma}{m_T} \mathbf{H} \mathbf{H}^H \right) \right), \quad (2)$$

where \mathbf{I} is an identity matrix of proper size, γ the signal to noise ratio (SNR), m_T the number of transmitting antennas, \mathbf{H} the channel matrix, and $\det(\cdot)$ denotes the determinant. Figure 5 shows the CDF of the capacity at an SNR of 10 dB. It can be observed that the array with DMN provides higher capacities. At an outage probability of 10 % (capacity CDF = 0.1) the array with DMN outperforms the array without DMN approximately by 7 % and the two element array by 13 %. The curve for the array with DMN is shifted to the right due to the improved antenna gain, while it has a steeper slope due to the higher diversity. The latter is a direct consequence of the lower values of the correlation coefficients. The 2-element array, on the other hand, has a curve with a less steep slope, as the diversity achievable with two antennas (although fairly uncorrelated) is much less significant.

3.2. Realistic Scenario

Figure 6 depicts a more realistic scenario. A fixed BS mounted at 10 m height employs a uniform circular array (UCA) consisting of 16 vertical dipole antennas. Two cars (MS₁, MS₂) mounting identical copies of the antenna array on their roofs move on the trajectories shown in the figure. Several clusters provide multi-path propagation, whereas two buildings introduce shadow fading. The MPC coming from the clusters are rather powerful, so that the Rician K -factor ranges between 3 and 6 in the LOS regions. The Rician K -factor is defined as the ratio between the power of the LOS and the power of the non LOS signals [9].

The downlink has been simulated by applying first the block diagonalisation (BD) algorithm proposed in [10, 11]. A single data stream has been sent to each MS, using strongest eigenmode transmission [9]. Thanks to the BD scheme, the

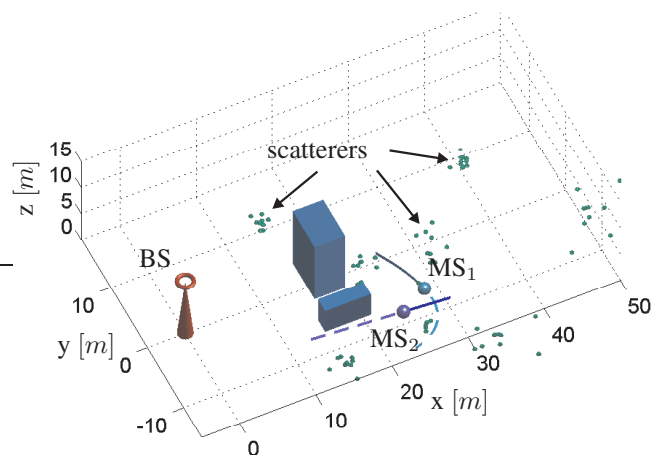


Fig. 6. Microcellular environment to test the 3-ULA with and without DMN. Several clusters of scatterers are placed around the mobiles while two buildings provide shadow fading.

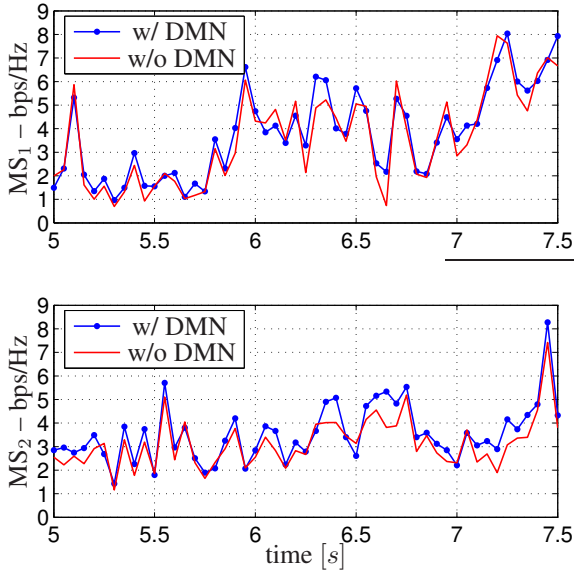


Fig. 7. User rates for the two users MS_1 and MS_2 mounting the array with and without DMN. The plot shows a representative time interval. The average SNR is 30 dB.

modulation vectors are chosen such that no interference is caused to the users. Maximum ratio combining (MRC) [12] has been performed at the receivers, assuming that perfect channel state information (CSI) is available at both the receiver and transmitter. The channels for both versions of the array with and without DMN have been computed.

Figure 7 shows the user rates for the two MS using the array with and without DMN. The plot shows only a representative time interval. It can be seen that for most of the time snapshots

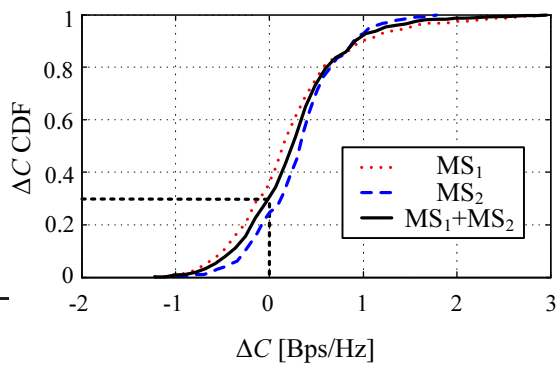


Fig. 8. CDF of the difference of the capacity ΔC obtained for the array with DMN and the one without. For approximately 70 % of the time snapshots the array with DMN achieves higher user rates. The average SNR is 30 dB.

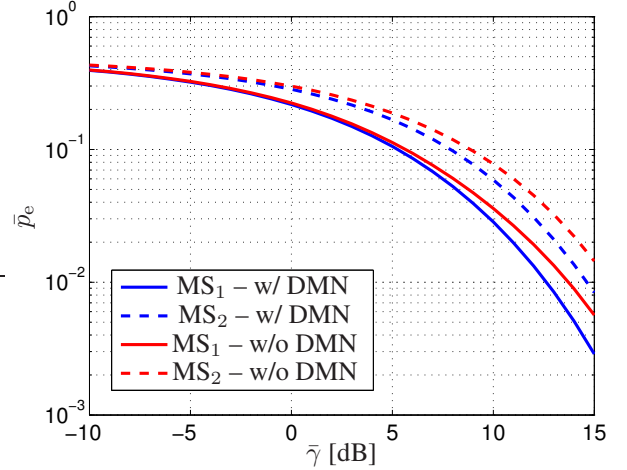


Fig. 9. Average BER \bar{p}_e versus average $\bar{\gamma}$ for the microcellular scenario in figure 6. We use BD with strongest eigenmode transmission and BPSK. At the receiver we assume MRC.

shots the array with DMN achieves higher user rates. However, in others, the array without DMN performs better. To investigate this more rigorously the difference of the capacity ΔC obtained for the array with and without DMN and its corresponding CDF has been computed and plotted in figure 8. Negative values of the abscissa represent time snapshots in which the array without DMN achieved a better rate. This happens in approximately 30 % of the cases. The maximum gain over the array with DMN is 1.3 bps/Hz. In the remaining 70 % of the cases the proposed array with DMN performs better, reaching a gain up to 3 bps/Hz.

This simulation shows that in a case where the MPCs arrive from a few specific directions, on average the proposed array with DMN is capable of achieving better user rates as it possesses higher gain and orthogonal beam patterns. The better performance of the array with the DMN can be observed also in the bit error rate (BER). Figure 9 shows the average BER curves for the microcellular scenario. As for the capacity curves, BD has been assumed with strongest eigenmode transmission at the transmitter, and MRC at the receiver. As transmission scheme binary phase-shift keying (BPSK) has been assumed. For a certain noise level which gives an average SNR $\bar{\gamma}$, the instantaneous SNR $\gamma(t)$ for each time snapshot t has been computed. The function $p_\gamma(\gamma)$ is the probability density function (PDF) of the instantaneous SNR. The BER $p_e(\gamma)$ for each SNR γ has been computed, obtaining the average BER, namely $\bar{p}_e(\bar{\gamma})$, by use of the following integral

$$\bar{p}_e(\bar{\gamma}) = \int_{-\infty}^{\infty} p_e(\gamma) \cdot p_\gamma(\gamma) d\gamma. \quad (3)$$

The plots show that the array with the DMN achieves better BER. In particular, the slope of the curves for the proposed array are steeper, indicating the higher diversity order.

4. DISCUSSION

Theoretically, within a narrow frequency band perfect matching and perfect orthogonalisation of the patterns can be achieved. In practice, the losses in the antennas and the DMN can lead to a degradation of the performance. This implies that the key point of this approach is a careful design of the DMN with respect to losses. The investigated $\lambda/4$ spaced monopole array is, even without DMN, an acceptable choice for MIMO applications. However, the proposed decoupling and matching can improve the array further.

By modelling the MPC explicitly, the IlmProp allows to create a scenario which approaches the assumptions in the theoretical model proposed by Jakes. In this case, the gains provided by the proposed array with respect to the version without DMN can be assessed quantitatively. The improvement is due to the higher array gain as well as to the higher diversity order which characterises the array. However, such a scenario is rather unrealistic, and therefore an environment has been modeled in which these arrays might actually be used. Within this microcellular scenario the arrays are mounted on two MS. By computation of the channels several investigations have been carried out, which confirm that the DMN improves the performance of the array also under realistic conditions.

5. CONCLUSIONS

We propose and evaluate a miniaturised 3-element antenna array featuring a decoupling and matching network (DMN). The latter effectively shapes the radiation patterns so that they are orthogonal to each other, i.e., they are pointed towards different sections of space. This leads to a higher antenna diversity which translates into higher capacity and lower bit error rate. The impact of the DMN is quantitatively evaluated by simulating the array with and without DMN by means of a geometry-based channel model.

ACKNOWLEDGEMENTS

We gratefully acknowledge the DLR (grant no. 50YB0509) for the partial financial support. We would also like to thank M. Huhn and M. Zocher for the technical assistance, and Ch. Kutscher for his assistance with the design and characterisation of the network elements.

REFERENCES

- [1] J. Weber, Ch. Volmer, K. Blau, R. Stephan, and M. A. Hein. Miniaturised antenna arrays using decoupling networks with realistic elements. In *IEEE Trans. Microwave Theory Tech.*, volume 54, pages 2733–2740, June 2006.
- [2] J. Weber, Ch. Volmer, K. Blau, R. Stephan, and M. A. Hein. Implementation of a miniaturised antenna array with predefined orthogonal radiation patterns. In *Proc. 1st European Conf. on Antennas and Prop. (EU-CAP'06)*, to be referenced in *IEEE Xplore*, Nice, France, November 2006.
- [3] High frequency laminates, Rogers Corporation, One Technology Drive, Rogers, CT 06263, USA.
- [4] G. Del Galdo, J. Lotze, M. Landmann, and M. Haardt. Modelling and manipulation of polarimetric antenna beam patterns via spherical harmonics. In *Proc. 14th European Signal Processing Conference (EUSIPCO)*, Florence, Italy, September 2006.
- [5] S. Stein. On cross coupling in multiple-beam antennas. *IEEE Trans. Antennas Propagat.*, AP10:548–557, September 1962.
- [6] R. G. Vaughan and J. Bach Andersen. Antenna diversity in mobile communications. *IEEE Trans. Veh. Technol.*, VT36:149–172, November 1987.
- [7] G. Del Galdo, M. Haardt, and C. Schneider. Geometry-based channel modelling of MIMO channels in comparison with channel sounder measurements. *Advances in Radio Science - Kleinheubacher Berichte*, pages 117–126, October 2003, more information on the model, as well as the source code and some exemplary scenarios can be found at <http://tu-ilmenau.de/ilmprop>.
- [8] W. C. Jakes, editor. *Microwave Mobile Communications*. IEEE Press, Piscataway, NJ, 1974.
- [9] A. Paulraj, R. Nabar, and D. Gore. *Introduction to space-time wireless communications*. Cambridge University Press, Cambridge, 2003.
- [10] Q. Spencer and M. Haardt. Capacity and downlink transmission algorithms for a multi-user MIMO channel. In *Proc. 36th Asilomar Conf. on Signals, Systems, and Computers*, Pacific Grove, CA, November 2002.
- [11] Q. H. Spencer, A. L. Swindlehurst, and M. Haardt. Zero-forcing methods for downlink spatial multiplexing in multiuser MIMO channels. *IEEE Transactions on Signal Processing*, 52, February 2004.
- [12] J. G. Proakis. *Digital Communications*. McGraw-Hill, Inc., University Press (Belfast), Ltd., 1995.